Journal of Catalysis **208,** 139–149 (2002)
doi:10.1006/jcat.2002.3570, available online at http://www.idealibrary.com on IDEAL®

Effect of Catalyst Structure on Oxidative Dehydrogenation of Ethane and Propane on Alumina-Supported Vanadia

Morris D. Argyle, Kaidong Chen, Alexis T. Bell,[1] and Enrique Iglesia[1]

Chemical and Material Sciences Divisions, Lawrence Berkeley National Laboratory; and Department of Chemical Engineering, University of California, Berkeley, California 94720-1462

Received September 20, 2001; revised February 9, 2002; accepted February 9, 2002

The catalytic properties of Al_2O_3-supported vanadia with a wide range of VO_x surface density (1.4–34.2 V/nm^2) and structure were examined for the oxidative dehydrogenation of ethane and propane. UV–visible and Raman spectra showed that vanadia is dispersed predominately as isolated monovanadate species below ∼2.3 V/nm^2. As surface densities increase, two-dimensional polyvanadates appear (2.3–7.0 V/nm^2), along with increasing amounts of V_2O_5 crystallites at surface densities above 7.0 V/nm^2. The rate constant for oxidative dehydrogenation (k_1) and its ratio with alkane and alkene combustion (k_2/k_1 and k_3/k_1, respectively) were compared for both alkane reactants as a function of vanadia surface density. Propene formation rates (per V atom) are approximately eight times higher than ethene formation rates at a given reaction temperature, but the apparent ODH activation energies (E_1) are similar for the two reactants and relatively insensitive to vanadia surface density. Ethene and propene formation rates (per V atom) are strongly influenced by vanadia surface density and reach a maximum value at intermediate surface densities (∼8 V/nm^2). The ratio of k_2/k_1 depends weakly on reaction temperature, indicating that activation energies for alkane combustion and ODH reactions are similar. The ratio of k_2/k_1 is independent of surface density for ethane but increases slightly with vanadia surface density for propane, suggesting that isolated structures prevalent at low surface densities are slightly more selective for alkane dehydrogenation reactions. The ratio of k_3/k_1 decreases markedly with increasing reaction temperature for both ethane and propane ODH. Thus, the apparent activation energy for alkene combustion (E_3) is much lower than that for alkane dehydrogenation (E_1) and the difference between these two activation energies decreases with increasing surface density. The lower alkene selectivities observed at high vanadia surface densities are attributed to an increase in alkene adsorption enthalpies with increasing vanadia surface density. The highest yield of alkene is obtained for catalysts containing predominantly isolated monovanadate species and operated at high temperatures that avoid homogeneous reactions (<∼800 K).

INTRODUCTION

Low-molecular-weight alkenes, such as ethene and propene, can be formed via nonoxidative dehydrogenation of the corresponding alkane. Nonoxidative dehydrogenation reactions are endothermic and lead to the concurrent formation of carbon and of lower molecular weight alkanes, both of which decrease alkene yields. Oxidative dehydrogenation (ODH) of light alkanes offers a potentially attractive route to alkenes, since the reaction is exothermic and avoids the thermodynamic constraints of nonoxidative routes by forming water as a by-product. In addition, carbon deposition during ODH is eliminated, leading to stable catalytic activity. However, the yield of alkenes obtained by ODH on most catalysts is limited by alkene combustion to CO and CO_2 (CO_x).

Previous studies have shown that supported vanadia is the most active and selective simple metal oxide for alkane ODH, because its reducible nature leads to the rapid redox cycles required for a catalytic turnover (1–5). Other studies (6–18) have probed the kinetics and selectivity of ethane and propane ODH on VO_x/Al_2O_3 and on VO_x species supported on other metal oxides. These studies have shown that ODH rates per gram of catalyst and alkene selectivities are higher on dispersed VO_x than on V_2O_5. The local structure of supported VO_x domains strongly influences ODH reaction rates and selectivity (12–14). The effects of oxide domain size and of support on rates and selectivity have been attributed to the acid–base properties of the VO_x and support surfaces (1–5, 7–18).

Alkane ODH reactions proceed via the reaction network shown in Scheme 1 (4, 10, 12–14, 19, 20), in which alkanes react with lattice oxygen to form alkenes, with a rate constant k_1, or CO_x, with a rate constant k_2. The alkenes formed undergo subsequent oxidation to CO_x with a rate constant k_3. Reaction rates are nearly zero order in O_2 and show a weak inhibition by H_2O formed in ODH reactions (14, 21). A pseudo-first-order kinetic analysis of Scheme 1 is sufficiently accurate to provide all three rate constants from rate and selectivity data as a function of

[1] To whom correspondence should be addressed. E-mail: iglesia@cchem.berkeley.edu; bell@cchem.berkeley.edu.

0021-9517/02 $35.00

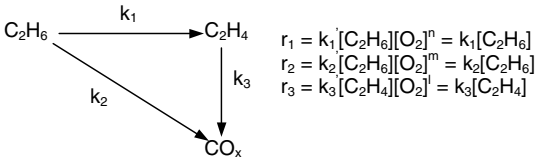

SCHEME 1

reactor residence time. High alkene yields at reasonable residence times require high values of k_1 and low values of k_2/k_1 and k_3/k_1.

The effects of VO_x surface density and structure on rates and selectivities for ethane and propane ODH reactions have been previously reported (7–18), with somewhat inconsistent results. For example, for ethane ODH on VO_x/γ-Al_2O_3 catalysts, the vanadia surface density that produces the highest ethane and ethene rates per V has been variously reported to occur at ~33 (9), ~50 (7), or ~70% (2) of the polyvanadate monolayer coverage. As another example, the variation of propene selectivity with vanadia surface density over a range of 1.7–3.9 V/nm^2 has been reported to be insignificant (2, 17) and quite significant, varying by ~20% (13), for propane ODH on VO_x/γ-Al_2O_3 catalysts. The lack of detailed structural characterization and rigorous kinetic analysis of integral (high conversion) rate and selectivity data, and the temperature gradients and possible homogeneous reactions prevalent at the high temperatures and conversions of many previous studies, have contributed to the persistent controversies.

Here, we report a detailed kinetic analysis of ethane ODH reactions on VO_x/Al_2O_3 samples with a wide range of VO_x surface densities (1.4–34 VO_x/nm^2) and contrast the results with those obtained using propane as the reactant. We have combined this analysis with detailed structural characterization of these catalysts in order to relate their local structure to the values of the rate constants, which characterize the function of these catalytic materials. In addition, we contrast the reaction rates of ethane and propane molecules with different C–H bond energies and different adsorption energies of the respective alkenes.

EXPERIMENTAL METHODS

VO_x/Al_2O_3 catalysts were prepared by incipient wetness impregnation of fumed γ-alumina (Degussa, AG, 100 m^2/g) with an aqueous solution of ammonium metavanadate (99%, Aldrich, Inc.) and oxalic acid (Mallinckrodt analytical grade) in a 1 : 2 weight ratio (12) with a pH of ~2. The impregnated samples were dried in air at 398 K for ~16 h, crushed, treated in 1.67 cm^3 s^{-1} (STP) dry air (Airgas zero grade) at 773 K for 3 h, and sieved to retain particles with diameters of 180–355 μm.

Surface areas were measured by N_2 physisorption (Airgas, 99.999%) at its normal boiling point using a Quantasorb surface area analyzer and standard multipoint BET analysis methods. The catalyst samples were treated in flowing He (Airgas, 99.999%) at 393 K for 2 h before N_2 physisorption measurements.

Diffuse reflectance UV–visible spectra were measured with a Varian–Cary 4 spectrophotometer equipped with a Harrick diffuse reflectance attachment. Samples were dehydrated in 20% O_2/He (1.67 cm^3 s^{-1}(STP), Praxair, 99.99%) at 723 K before measuring spectra at ambient temperature between 1 and 5 eV. The Kubelka–Munk function ($F(R_\infty)$) was used to convert diffuse reflectance data into absorption spectra using MgO as a standard (22). The absorption edge energy was estimated from the x-intercept of a linear fit in the near-edge region in a plot of $(F(R_\infty)h\nu)^{1/2}$ as a function of $h\nu$ (22).

Raman spectra were obtained using a Hololab Series 5000 Raman spectrometer (Kaiser Optical) with a frequency-doubled 75-mW Nd-YAG laser at a wavelength of 532 nm. VO_x/Al_2O_3 samples (~0.05 g) were pressed into wafers (0.9-cm diameter, ~0.1-cm thickness) at 40 MPa and Raman spectra were measured at ambient temperatures before and after dehydration treatments. Dehydration was carried out at 723 K in flowing 20% O_2 (Airgas, 99.99%) in He (Scott Specialty Gases, Inc., 99.9999%) at a total flow rate of 1.0 cm^3 s^{-1} (STP) for 0.75 h. A rotating Raman cell (20 Hz) was used to prevent laser heating of the samples (23).

Reaction rate and selectivity data were measured in a packed-bed flow reactor with plug-flow hydrodynamics (24). VO_x/Al_2O_3 catalysts (0.01–0.3 g) were diluted with quartz granules (180- to 355-μm diameter, 0.01–0.3 g) in order to prevent bed temperature gradients. Reaction measurements with Al_2O_3, quartz chips, or empty reactors did not lead to detectable products in the temperature range of the study. Typical propane and O_2 conversion ranges on VO_x/Al_2O_3 catalysts were 1–2 and 10–20%, respectively. A Hewlett–Packard 6890 gas chromatograph equipped with packed (Supelco Carboxen 1004) and capillary (HP-1, 50 m, 320 μm) columns and thermal conductivity and flame ionization detectors was used to measure the concentrations of reactants and products in the effluent stream.

Ethane ODH reactions were examined at 663–743 K, while the faster propane ODH reactions were examined at lower temperatures (603–663 K). No homogeneous ethane or propane reactions were detected below 800 K. Reactor residence times were adjusted by varying reactant flow rates between 0.083 and 4.2 cm^3 s^{-1} (STP). Reactant mixtures consisted of ethane (14 kPa, Scott Specialty Gases, Inc., 99.999%) or propane (14 kPa, Airgas, 99.9%) with O_2 (1.7 kPa, Praxair, 99.999%) and He as an inert diluent (Airgas, 99.9999%).

Conversion and selectivity were calculated from the measured GC compositions. These data were used to calculate reaction rates from the reactant and product molar flow rates. The reaction rates and selectivities as a function of residence time were used to obtain initial alkane dehydrogenation and combustion reaction rates and the rate constants shown in Scheme 1. The sequence in Scheme 1 can be used to obtain the k_1 and k_2 rate constants from the initial alkene selectivity,

$$S^0_{\mathrm{CxH2x}} = k_1/(k_1 + k_2),$$

and k_3 from the observed changes in alkene selectivity with residence time,

$$S_{\mathrm{CxH2x}} = S^0_{\mathrm{CxH2x}}[1 - (k_1 + k_2 + k_3)C_{\mathrm{V}}\tau/2],$$

where τ is residence time and C_{V} is the concentration of V atoms per reactor volume, as described in detail elsewhere (12).

RESULTS AND DISCUSSION

Catalyst Characterization

BET surface areas and apparent VO_x surface densities, estimated from the V content and the BET surface areas, are shown in Table 1 for all VO_x/Al_2O_3 samples. Surface areas (per gram of sample) decrease with increasing VO_x content. This trend corresponds to the low surface area of the added VO_x because the surface area normalized per alumina content, listed in the last column of Table 1, is approximately constant. However, the 30 wt% sample shows a decrease in surface area per gram of alumina, suggesting that the formation of larger V_2O_5 crystallites blocks some support pores.

The UV–visible spectra and the absorption edge energies for all VO_x/Al_2O_3 samples are shown in Figs. 1a and 1b, respectively. VO_x/Al_2O_3 samples with 8.0, 12.5, 16.6, and 34.2 V/m^2 exhibit two linear regions in the near-edge region, indicating the presence of two distinct VO_x structures. For those samples, two edge energies are measured and both are included in Fig. 1b. The low-energy absorption edge decreases in energy with increasing surface density, approaching values typical of bulk V_2O_5 (2 eV) (25). The edge energies based on the second linear portion of the near-edge region are higher than those based on the first linear portion and appear to be independent of the vanadia surface density. Absorption edge energies above 2.5 eV are attributable to V^{5+} in distorted tetrahedral

TABLE 1

Surface Area and V Surface Density for VO_x/Al_2O_3 Catalysts

V_2O_5 loading (wt%)	Surface area (m^2/g)	Nominal VO_x surface density (V/nm^2)	Surface area normalized by amount of support (m^2/g Al_2O_3)
0	99	0	99
2	95	1.4	97
5	93	3.6	97
10	83	8.0	92
15	80	12.5	94
20	73	16.6	91
30	58	34.2	83

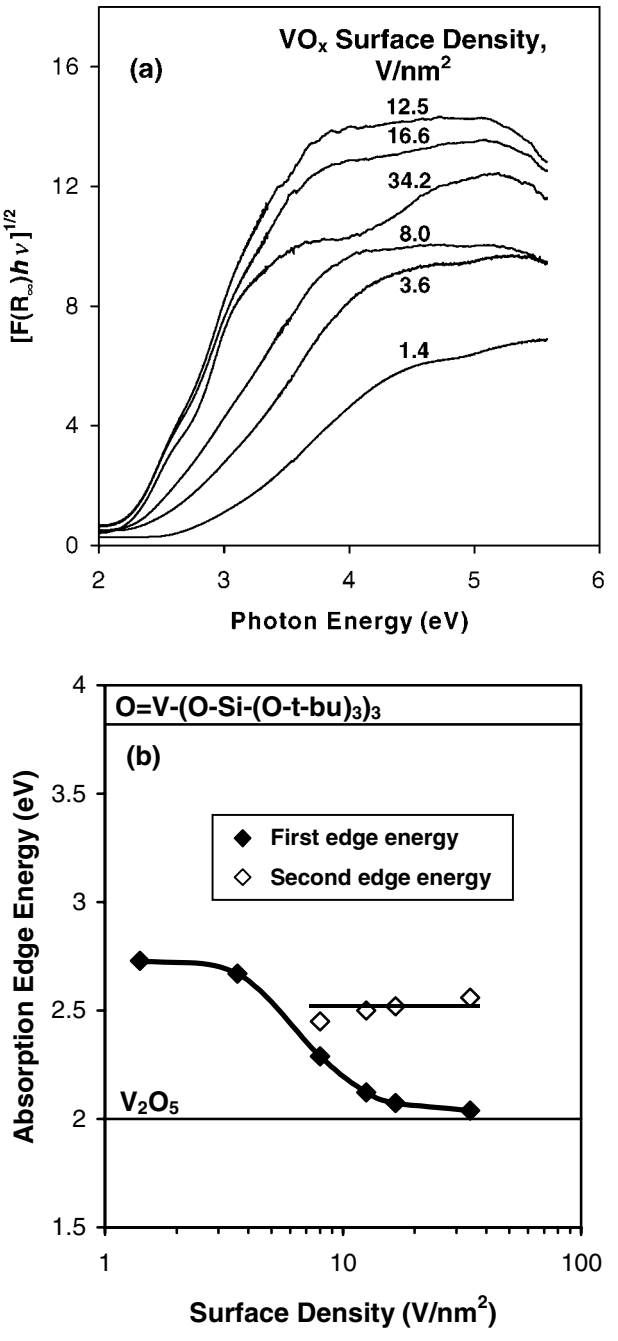

FIG. 1. (a) Diffuse reflectance UV–visible spectra and (b) absorption edge energies for VO_x/Al_2O_3 catalysts.

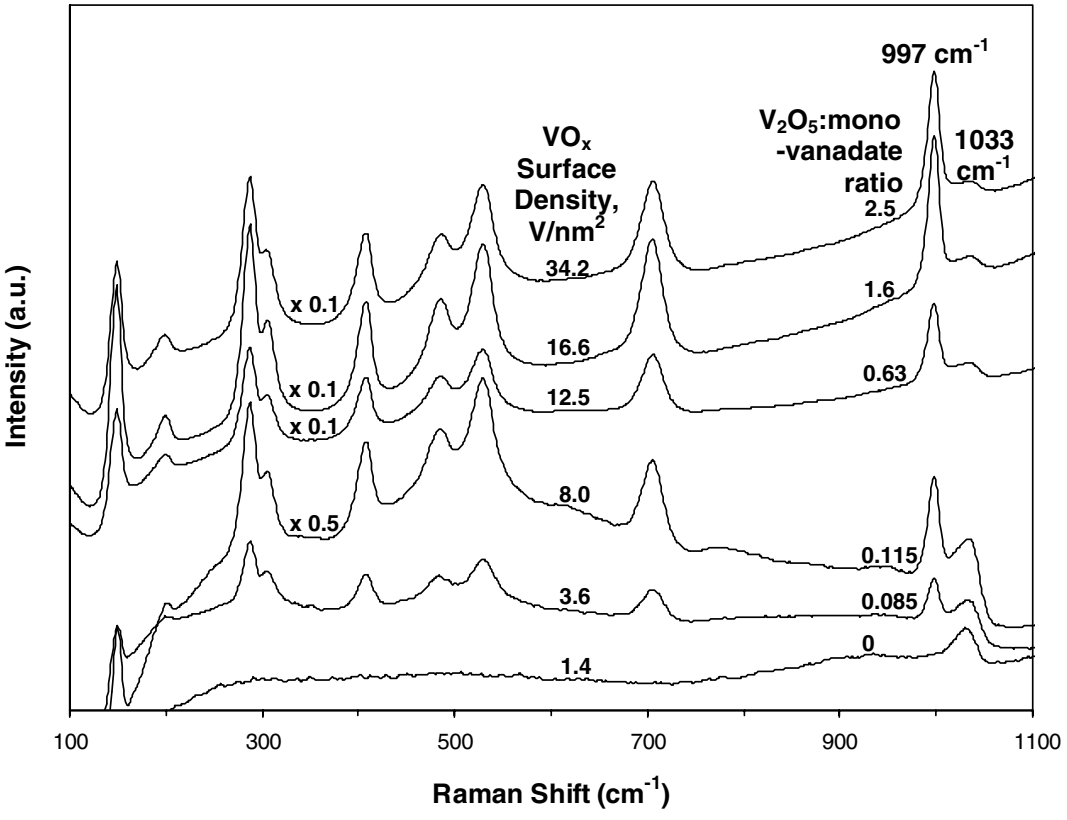

FIG. 2. Raman spectra for VO_x/Al_2O_3 catalysts (obtained at 298 K in flowing dry 20% O_2/He after treatment at 723 K for 0.75 h).

coordination (25). Thus, UV–visible spectroscopy suggests that V^{5+} is present in distorted tetrahedrally coordinated species at low vanadia surface densities and that some of these tetrahedrally coordinated cations remain at higher surface densities, coexisting with an increasing fraction of V^{5+} present in distorted tetragonal pyramidal coordination, similar to that present in V_2O_5 (25).

Raman spectra, obtained at ambient temperature after treatment at 723 K in 20% O_2/He, for the VO_x/Al_2O_3 samples are shown in Fig. 2. V=O stretches in isolated tetrahedral monovanadates appear at 1033 cm^{-1}, while V–O–V stretches in two-dimensional polyvanadates have been proposed to lead to broad Raman features at 750–1000 cm^{-1} (25–27). The remaining bands, appearing at 998, 706, 530, 489, 410, 305, 289, 203, and 150 cm^{-1}, correspond to bulk V_2O_5 crystals (1, 25). The V_2O_5 bands in some of these spectra are intense, but the Raman cross section for V_2O_5 crystals is about 10 times larger than for monovanadate species (23). Using this value, the ratio of V atoms in V_2O_5 to those in monovanadate increases from 0 to 2.5 as VO_x surface densities increase from 1.4 to 34.2 V/nm^2. Geometric calculations, assuming flat, ordered support surfaces, predict that a theoretical monolayer of monovanadate species occurs at 2.3 V/nm^2, and at 7.0 V/nm^2 if polyvanadate species are present (12, 28). Over this range of VO_x surface densities, the ratio of V_2O_5 to monovanadate species increases from ~0.02 to ~0.1. Thus, under either definition of a monolayer, most of the surface is covered by vanadate species other than V_2O_5. Specifically, the V_2O_5 : monovandate ratio increases from 0.085 for the catalyst with a vanadia surface density of 3.6 V/nm^2 to 0.115 for the catalyst with a vanadia surface density of 8.0 V/nm^2. This represents an increase of 35% in the ratio of V_2O_5 to monovanadate species at the same time that the vanadia concentration doubled, indicating that the additional vanadia formed structures that are neither isolated monovanadates nor V_2O_5 crystallites. The V_2O_5 : monovandate ratio increases to 0.63, 1.6, and 2.5 for the catalysts with vanadia surface densities of 12.5, 16.6, and 32.4 V/nm^2, which have vanadia concentrations of 15, 20, and 30 wt%, respectively. The increase in the V_2O_5:monovadate ratio is proportionally larger than the additional vanadia content of these catalysts, suggesting that all added vanadia forms V_2O_5 structures while simultaneously incorporating some monovanadates.

The spectroscopic results presented in Figs. 1 and 2 suggest that distorted tetrahedral monovanadate structures connected to the support via V–O–Al bonds are prevalent at low surface densities. As V surface densities increase, two-dimensional polyvanadates form via reactions leading to V–O–V bonds connecting neighboring VO_x species. VO_x species exceeding monolayer coverages react with polyvanadates structures to form three-dimensional structures

that ultimately crystallize into bulk V_2O_5, with some evidence for residual monovanadate species.

Oxidative Dehydrogenation Rates and Selectivity

C_2H_4, CO, and CO_2 formation rates, C_2H_6 conversion level, and C_2H_4, CO, and CO_2 selectivities are shown as a function of nominal reactor residence time in Figs. 3a and 3b for the 8.0 V/nm^2 sample. The lines shown were used to extrapolate rates and selectivity to zero reactor residence time or reactant conversion and to estimate the rates of secondary oxidation of C_2H_4. The decrease in C_2H_6 conversion rates with increasing residence time (Fig. 3a) reflects a slight inhibition of ethane dehydrogenation rates by the water formed during reaction (21), as reported previously for propane reactions (14, 29, 30). The decrease in ethene selectivity with increasing residence time (Fig. 3b) arises from secondary ethene oxidation reactions (Scheme 1). Data acquisition methods similar to those described for ethane ODH were used to obtain the propane ODH data. The conversion and selectivity trends displayed in Fig. 3 for ethane ODH are similar to those observed for propane ODH, as described in more detail elsewhere (13, 14).

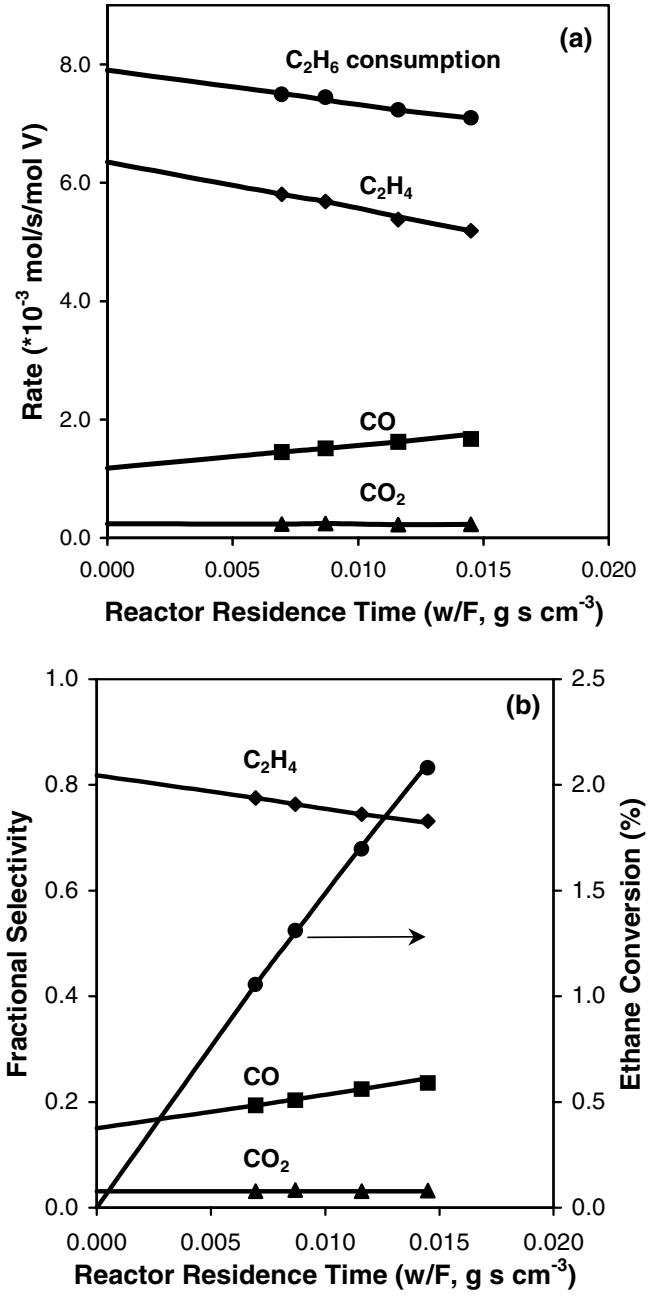

FIG. 3. Example of ethane ODH (a) reaction rates and (b) selectivity and conversion as a function of reciprocal flow rate (10% V_2O_5/Al_2O_3, 723 K, 14 kPa C_2H_6, 1.7 kPa O_2, balance He).

Figures 4a and 4b show the effect of vanadia surface density on the initial rate of alkene formation per V atom (extrapolated to zero residence time). For both ethane and propane reactants, these apparent turnover rates reach a maximum at intermediate vanadia surface densities. The maximum rate is reached at a surface VO_x density of ~8 V/nm^2 for both reactants, and this maximum rate is about four times greater than that obtained on the VO_x/Al_2O_3 sample with the lowest surface density (1.4 V/nm^2). Well-dispersed monovanadate species prevalent in the latter sample are significantly less active than the oligomeric VO_x structures that appear as the vanadia surface density increases. The rate per V atom increases with surface densities, even though V atoms become increasingly unavailable for catalysis as three-dimensional structures form. Thus, the surface reactivity of VO_x increases even more markedly with surface density than is suggested by the data in Fig. 4. For a given VO_x surface density, the apparent turnover rates for propane reactants is approximately eight times higher than for ethane, but the effects of vanadia surface density and the higher surface reactivity of the VO_x oligomers are observed for both alkane reactants.

Figures 4a and 4b show that apparent turnover rates for both ethane and propane decrease at VO_x surface densities above ~8 V/nm^2, as also found previously for propane ODH on VO_x/ZrO_2 (31). These trends reflect the introduction of additional vanadia species within the inaccessible bulk of three-dimensional structures. The picture of the sample surfaces evolving from isolated and sparsely distributed monovanadates, to nearly complete polyvanadate monolayers, followed by the gradual building of additional layers would lead to low areal ODH rates at low surface densities, because most of the surface area is inactive Al_2O_3. The increasing coverage of the Al_2O_3 with monovanadate and with more reactive polyvanadates would increase the measured areal rates, until the entire surface was covered with VO_x species. If the surface reactivity of such species becomes independent of the presence and scale of the third dimension, the areal rates would reach a constant value. These

trends are confirmed by the areal rates of alkene formation from ethane or propane, plotted as a function of vanadia surface density in Figs. 5a and 5b. These areal rates increase with increasing surface density and approach nearly constant values for vanadia surface densities higher than 10 V/nm^2, as also found for propane ODH on VO_x/ZrO_2 (31). The constant areal rate obtained after completion of a polyvanadate monolayer suggests that the surface reactivity of VO_x species becomes independent of domain size once the predominant structures involve V–O–V bonds.

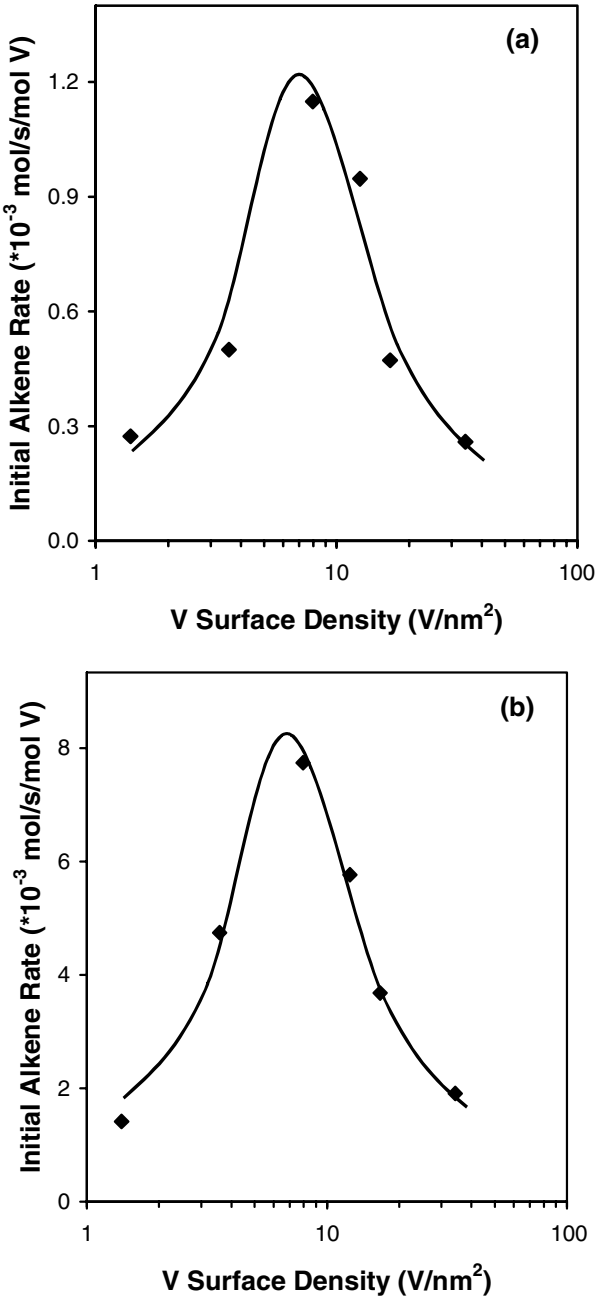

FIG. 4. Initial alkene formation rates as a function of vanadia surface density on VO_x/Al_2O_3 catalysts: (a) ethane ODH, (b) propane ODH (663 K, 14 kPa C_2H_6 or C_3H_8, 1.7 kPa O_2, balance He).

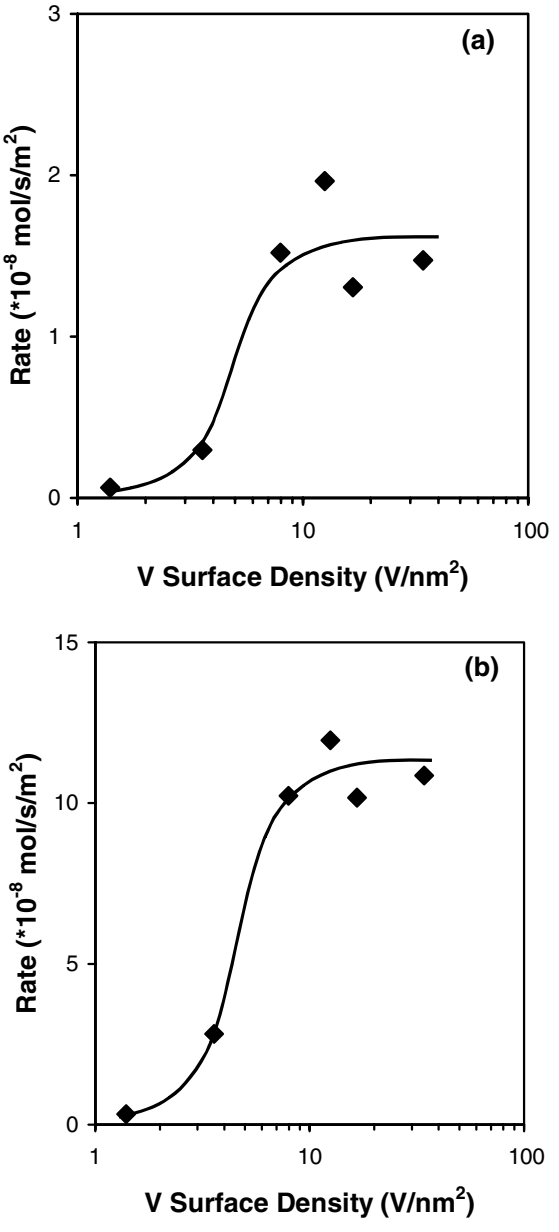

FIG. 5. Initial alkene formation rates normalized per unit catalyst surface area as a function of vanadia surface density: (a) ethane ODH, (b) propane ODH (663 K, 14 kPa C_2H_6 or C_3H_8, 1.7 kPa O_2, balance He).

Figure 6 shows activation energies (E_1) obtained from Arrhenius plots for ethene and propene formation rates from the corresponding alkanes as a function of VO_x surface density. Ethane and propane dehydrogenation show similar activation energies, and the value decreases slightly for both reactants with increasing VO_x surface density. Similar and even lower values of E_1 than those presented in Fig. 6 have been reported for ethane ODH on VO_x/Al_2O_3

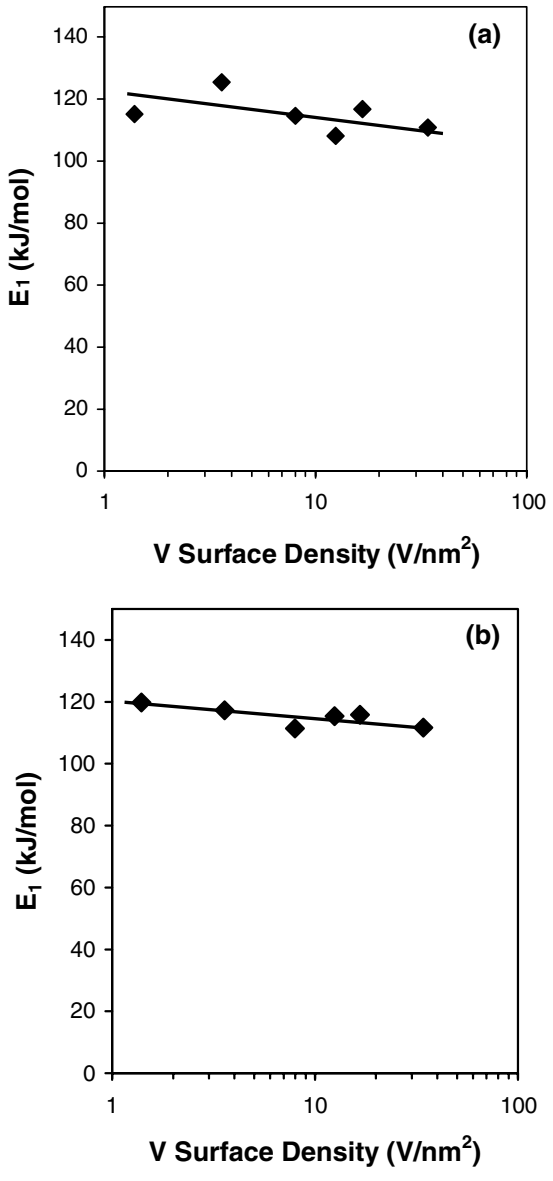

FIG. 6. ODH reaction activation energy, E_1, as a function of vanadia surface density on VO_x/Al_2O_3 catalysts: (a) ethane, (b) propane (14 kPa alkane, 1.7 kPa O_2, balance He).

(7). The similar values of E_1 of the two reactants is unexpected, because propane dehydrogenation is significantly faster than ethane dehydrogenation. Since C–H bond activation is the kinetically relevant step in dehydrogenation of propane (1–4, 12, 14, 19, 29 30) and also ethane on vanadia-based catalysts (19), and the methylene C–H bonds in propane are considerably weaker than the methyl C–H bonds in ethane (401 vs 420 kJ/mol), a lower activation energy is expected for propane than for ethane dehydrogenation reactions. Therefore, other factors must account for the equivalence of the activation energies for ethane and propane ODH. One of these factors may be the stability of the alkyl radical formed upon C–H bond activation. A higher stabilization energy for ethoxide species relative to isopropoxide species could compensate for the differences in C–H bond energies in the transition state involved in C–H bond activation and lead to similar activation energies for the two alkane reactants.

Dehydrogenation rates are much lower for ethane than for propane (Fig. 4) even though activation energies are similar (Fig. 6). This means that either the number of active sites or the preexponential factor must be much lower for ethane than for propane reactants. It appears unlikely that the mechanism or site requirements would differ for two alkanes as similar as propane and ethane, which react via similar redox mechanisms using lattice oxygen atoms (1–5, 12, 14, 21, 29, 30). The lower preexponential factors would then have to reflect a larger negative entropy of formation of the transition state for ethane than for propane. An analysis based on transition state theory and on the expected structures of activated complexes required for C–H bond activation, however, does not indicate that the activation entropy of ethane ODH is more negative than that of propane ODH. These theoretical considerations suggest that activation entropy differences do not explain the higher rate of propane ODH relative to ethane ODH.

Figure 7 illustrates the effect of VO_x surface density on alkene selectivities. The initial selectivity to ethene is ~75% for ethane ODH on VO_x/Al_2O_3 and it does not change significantly with increasing VO_x surface density (Fig. 7a). CO is the major by-product and only a small amount of CO_2 is formed. For propane ODH reactions, initial propene selectivities are ~85% at the lowest vanadia surface densities, but they decrease to values similar to those for ethane reactants with increasing surface density (Fig. 7b).

The ratios of rate constants for alkane direct combustion and dehydrogenation (k_2/k_1) are shown in Fig. 8 as a function of VO_x surface density. For ethane, k_2/k_1 is essentially independent of VO_x surface density, but this ratio increases with increasing VO_x surface density for propane reactants. For ethane, k_2/k_1 is weakly dependent on temperature, while for propane, k_2/k_1 is essentially independent of temperature on all samples, indicating that the activation energies for alkene and CO_x formation directly from alkanes (E_1 and E_2) are very similar (Fig. 9). The differences between these two activation energies ($\Delta E_{12} = E_1 - E_2$) are small, positive, and independent of VO_x surface density for ethane, but change from positive to negative with increasing VO_x surface density for propane ODH. These trends are consistent with the observed trends in k_2/k_1 shown in Fig. 8.

Figure 10 shows ratios of rate coefficients for alkene combustion and alkane dehydrogenation (k_3/k_1). For both reactants, k_3/k_1 increases with increasing VO_x surface density and decreases with increasing temperature on all samples. This is consistent with a lower activation energy for alkene reactions (E_3) than for alkane reactions (E_1). This

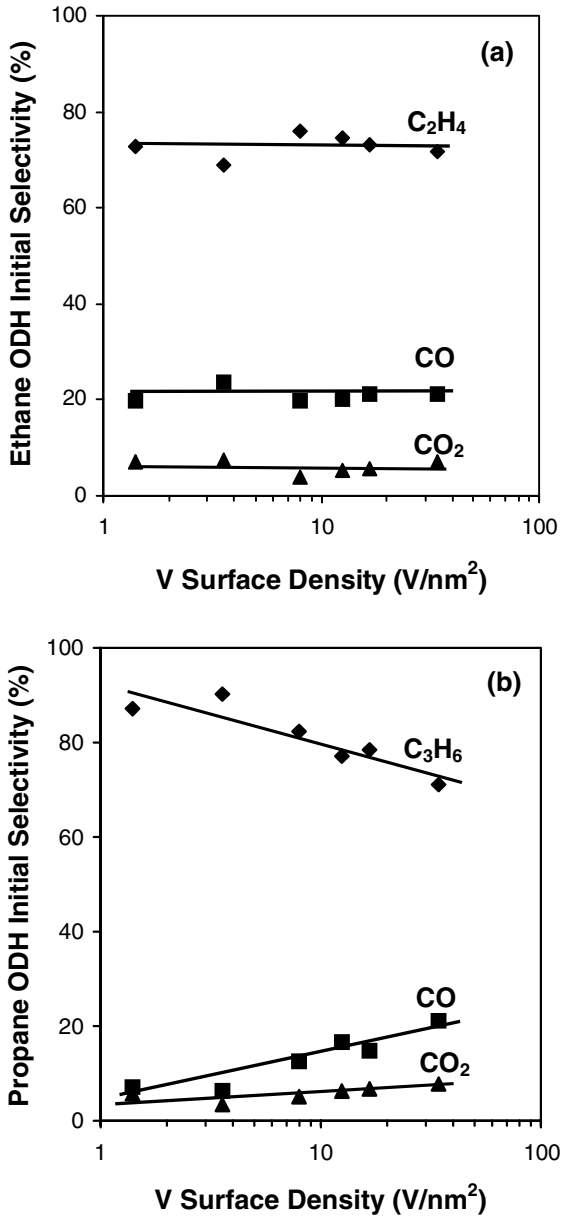

FIG. 7. ODH selectivities as a function of vanadia surface density on VO_x/Al_2O_3 catalysts: (a) ethane, (b) propane (663 K, 14 kPa alkane, 1.7 kPa O_2, balance He).

activation energy difference ($\Delta E_{13} = E_1 - E_3$) decreases for both alkanes with increasing VO_x surface density (Fig. 11), consistent with trends shown in Fig. 10. E_1 values decrease very slightly with increasing surface density; thus, the observed changes in ΔE_{13} arise almost exclusively from an increase in the value of E_3 with increasing VO_x surface density.

Changes in alkene adsorption enthalpies may account for the observed increase in alkene combustion activation energies (E_3) with increasing vanadia surface density. Theoretical estimates of enthalpies for ethene adsorption on supported polyvanadate monolayers ($V_2O_5(001)/TiO_2(001)$ (anatase)) and bulk $V_2O_5(001)$ surfaces (32) give values of -79.6 and -39.7 kJ/mol, respectively. These density functional theory calculations are consistent with a higher activation energy on the bulk V_2O_5 surface, which binds ethene much more weakly than two-dimensional VO_x structures. This is apparent from the definition of k_3 as $K_3 k_3^{act}$, where K_3 is the equilibrium constant for ethene adsorption and k_3^{act} is the rate constant for the activation of a C–H bond in ethene. Thus, the apparent activation energy is given by $\Delta H_3 + E_3^{act}$, where ΔH_3 is the ethene adsorption enthalpy

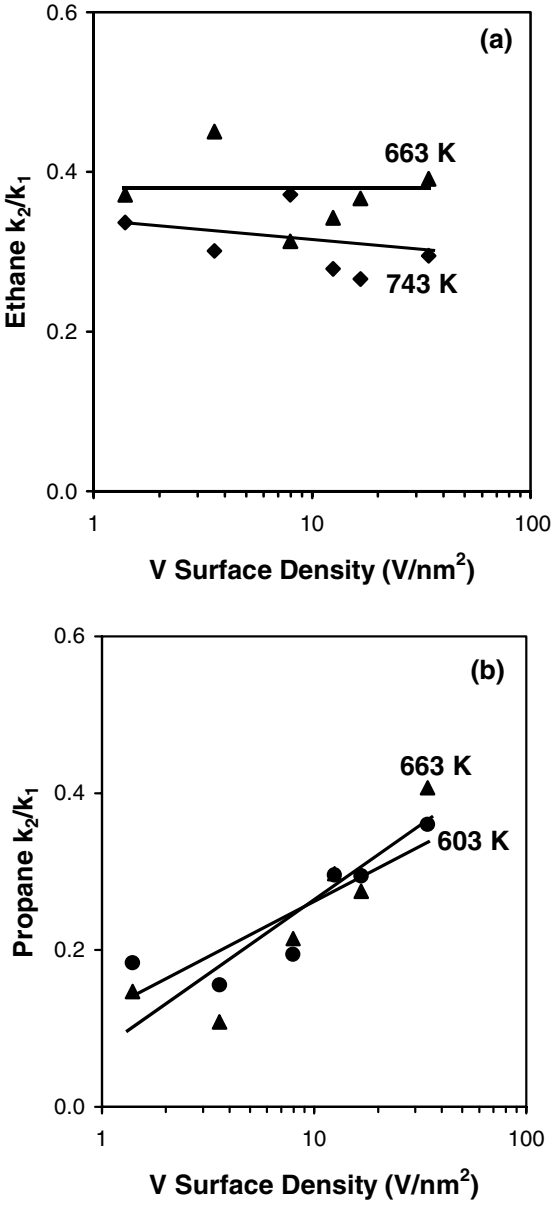

FIG. 8. Rate constant ratio k_2/k_1 as a function of vanadia surface density on VO_x/Al_2O_3 catalysts: (a) ethane (14 kPa C_2H_6, 1.7 kPa O_2, balance He), (b) propane (14 kPa C_3H_8, 1.7 kPa O_2, balance He).

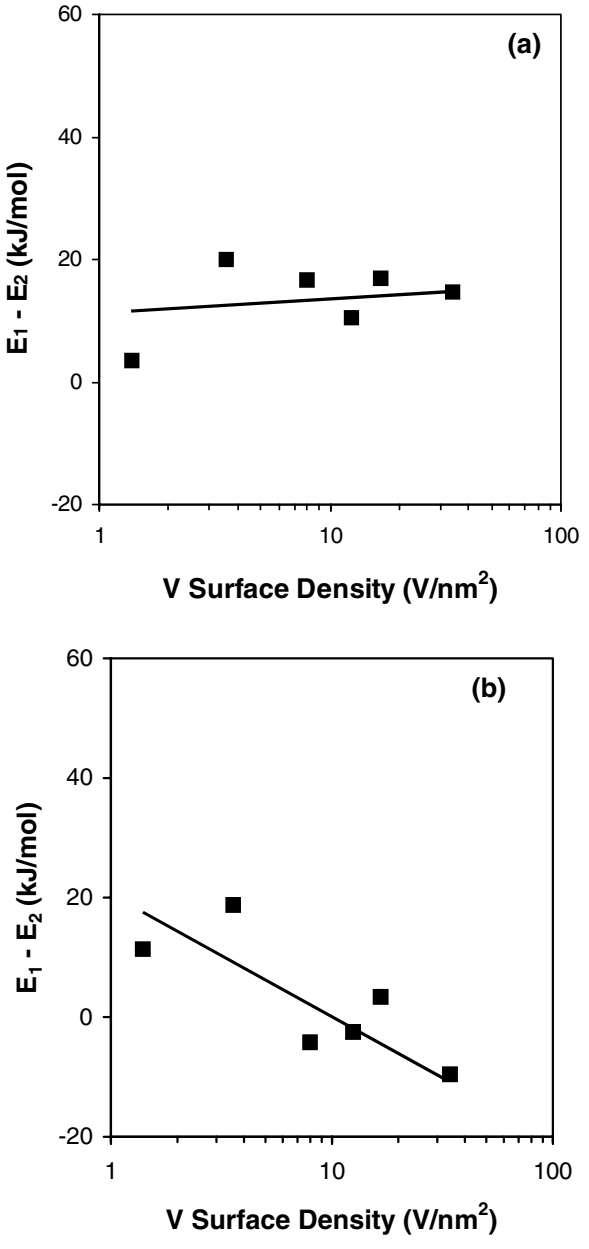

FIG. 9. Difference between ODH activation energy and alkane combustion activation energy ($\Delta E_{12} = E_1 - E_2$) on VO_x/Al_2O_3 catalysts: (a) ethane (663 K, 14 kPa C_2H_6, 1.7 kPa O_2, balance He), (b) propane (663 K, 14 kPa C_3H_8, 1.7 kPa O_2, balance He).

and E_3^{act} is the activation energy for the kinetically relevant C–H bond activation step in adsorbed ethene (29). The enthalpy of adsorption of ethane is not very sensitive to VO_x surface structure (−27.4 kJ/mol on $V_2O_5(001)/TiO_2$ and −25.4 kJ/mol on $V_2O_5(001)$ (32)). Taken together with the nearly constant values of E_1 (Fig. 6) on VO_x/Al_2O_3 samples with a wide range of surface density, this suggests that the energy for C–H bond activation in ethane (E_1^{act}) is not influenced by vanadia surface density. The mechanistic and kinetic resemblance between C–H bond activation steps in alkanes and alkenes and the different observed sensitivities of E_1 and E_3 on surface density suggest that only the adsorption enthalpy of alkenes, not that of alkanes and not the values of C–H bond activation energies (E_1^{act}, E_3^{act}), change with VO_x surface density.

The sample with the lowest vanadia surface density (1.4 V/nm^2) and containing predominately monovanadates shows the highest initial alkene selectivity for both ethane and propane ODH. Increasing vanadia surface density either has no effect or decreases initial alkene selectivities.

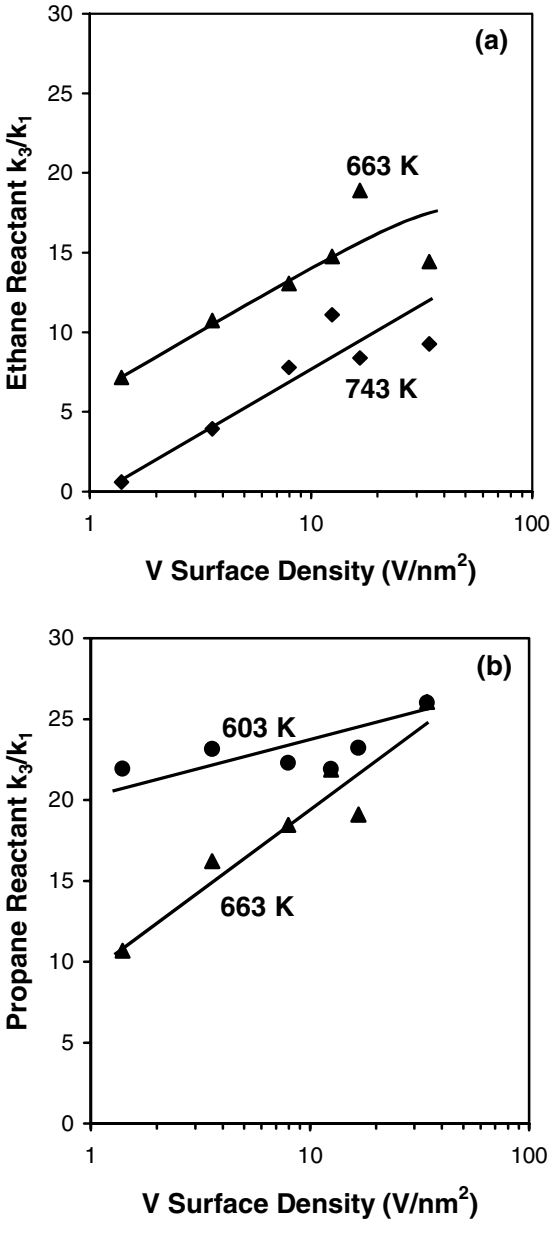

FIG. 10. Rate constant ratio, k_3/k_1, as a function of vanadia surface density on VO_x/Al_2O_3 catalysts: (a) ethane reactant (14 kPa C_2H_6, 1.7 kPa O_2, balance He), (b) propane reactant (14 kPa C_3H_8, 1.7 kPa O_2, balance He).

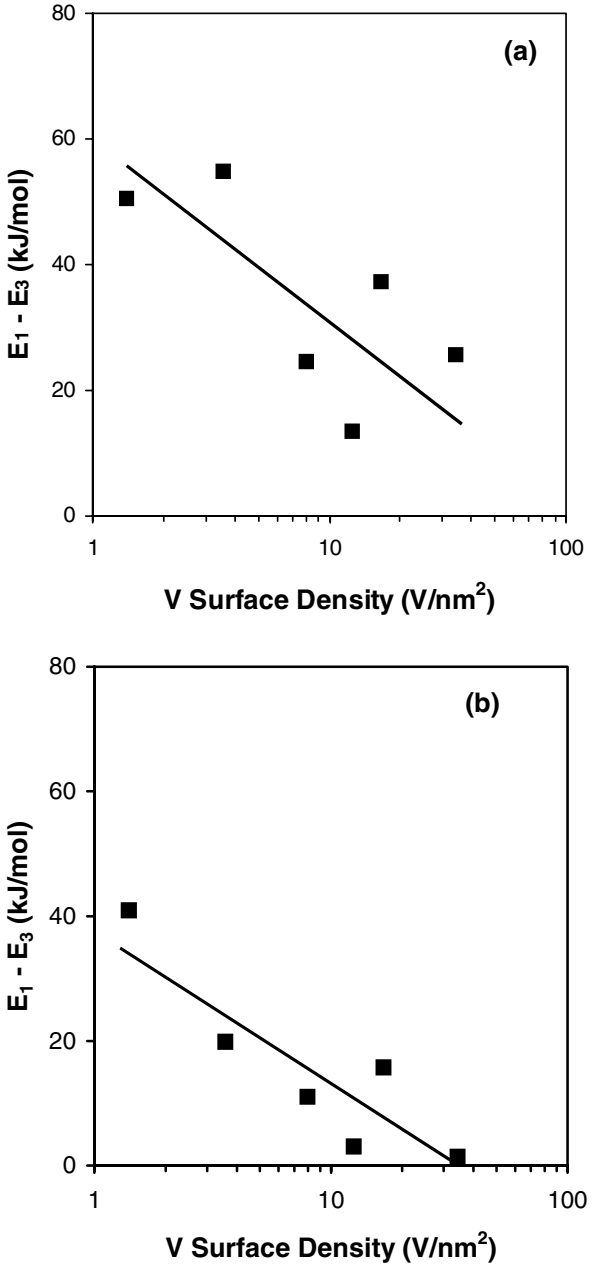

FIG. 11. Difference between ODH activation energy and alkene combustion activation energy ($\Delta E_{13} = E_1 - E_3$) on VO_x/Al_2O_3 catalysts: (a) ethane (663 K, 14 kPa C_2H_6, 1.7 kPa O_2, balance He), (b) propane (663 K, 14 kPa C_3H_8, 1.7 kPa O_2, balance He).

The ratio of k_2/k_1 is independent of surface density for ethane and increases with increasing vanadia surface density for propane (Fig. 8). The ratio of k_3/k_1 increases with increasing vanadia surface density for both reactants (Fig. 10). Smaller values of k_3/k_1 and k_2/k_1 lead to higher alkene selectivity at all reactant conversion levels. As a result, the 1.4 V/nm^2 catalyst is the most selective for both alkanes. However, the alkene formation rates (per V atom) for the 1.4 V/nm^2 catalyst are approximately four times lower at a given reaction temperatures compared to the 8.0 V/nm^2 catalyst (Fig. 4), but the rate difference can be overcome by increasing reaction temperatures. The ratio of k_2/k_1 is relatively independent of reaction temperature, and the value of k_3/k_1 actually decreases with increasing temperature for both reactants, leading to an increase in alkene selectivity with increasing reaction temperature. Therefore, the alkene yield can be maximized using a catalyst covered with dispersed monovanadate species, operated at high reaction temperature. The maximum operating temperature is determined by the onset of homogeneous reactions.

CONCLUSIONS

The rate and selectivity of ethane and propane ODH on VO_x/Al_2O_3 catalysts depend on the vanadia surface densities and reaction temperature. Ethane ODH at zero conversion is ~75% selective to ethene and insensitive to vanadia surface density, while initial propene selectivities during propane ODH approach 90% at low vanadia surface densities, but decrease with increasing vanadia surface density. The ratio of k_2/k_1 is relatively independent of both reaction temperature and vanadia surface density for ethane ODH. The ratio of k_2/k_1 is independent of reaction temperature, but increases with increasing vanadia surface density for propane ODH. However, k_3/k_1 is generally higher for propane than for ethane ODH, indicating that the propene is more reactive relative to propane than ethene is to ethane. The activation energies for ethane and propane ODH, E_1, and ethane and propane combustion, E_2, are similar in magnitude at $\sim 115 \pm 20$ kJ/mol and show weak dependence on vanadia surface density. The propene formation rate is approximately eight times larger than the ethene formation rate at 663 K, suggesting that that the stabilization energy for ethoxide species may be higher relative to isopropoxide in the activated state. The apparent activation energy for alkene combustion, E_3, is ~60–90 kJ/mol and increases with vanadia surface density, leading to a decrease in ΔE_{13} with increasing vanadia surface density. The trends in E_3 and ΔE_{13} appear to be caused by decreasingly exothermic alkene adsorption as vanadia surface density increases. Alkene selectivity generally increases with increasing reaction temperature and with decreasing vanadia surface density. Therefore, the highest olefin yields are obtained on catalysts containing isolated monovanadates and operated at the highest possible reaction temperature consistent with the avoidance of homogeneous reactions.

ACKNOWLEDGMENT

This work was supported by the Director, Office of Basic Energy Sciences, Chemical Sciences Division of the U.S. Department of Energy under Contract DE-AC03-76SF00098.

REFERENCES

1. Kung, H. H., *Adv. Catal.* **40**, 1 (1994).
2. Mamedov, E. A., and Cortés Corberán, V., *Appl. Catal. A* **127**, 1 (1995).
3. Albonetti, S., Cavani, F., and Trifirò, F., *Catal. Rev.–Sci. Eng.* **38**, 413 (1996).
4. Blasco, T., and López Nieto, J. M., *Appl. Catal. A* **157**, 117 (1997).
5. Bañares, M. A., *Catal. Today* **51**, 319 (1999).
6. Thorsteinson, E. M., Wilson, T. P., Young, F. G., and Kasai, P. H., *J. Catal.* **52**, 116 (1978).
7. Le Bars, J., Auroux, A., Forissier, M., and Vedrine, J. C., *J. Catal.* **162**, 250 (1996).
8. Le Bars, J., Vedrine, J. C., Auroux, A., Trautmann, S., and Baerns, M., *Appl. Catal. A* **119**, 341 (1994).
9. Bañares, M. A., Gao, X., Fierro, J. L. G., and Wachs, I. E., *Stud. Surf. Sci. Catal.* **110**, 295 (1997).
10. Blasco, T., Galli, A., López Nieto, J. M., and Trifiró, F., *J. Catal.* **169**, 203 (1997).
11. Gao, X., Banares, M. A., and Wachs, I. E., *J. Catal.* **188**, 325 (1999).
12. Khodakov, A., Yang, J., Su, S., Iglesia, E., and Bell, A. T., *J. Catal.* **177**, 343 (1998).
13. Khodakov, A., Olthof, B., Bell, A. T., and Iglesia, E., *J. Catal.* **181**, 205 (1999).
14. Chen, K. D., Khodakov, A., Yang, J., Bell, A. T., and Iglesia, E., *J. Catal.* **186**, 325 (1999).
15. Arena, F., Frusteri, F., and Parmaliana, A., *Catal. Lett.* **60**, 59 (1999).
16. Corma, A., López-Nieto, J. M., Paredes, N., Pérez, M., Shen, Y., Cao, H., and Suib, S. L., *Stud. Surf. Sci. Catal.* **72**, 213 (1992).
17. Eon, J. G., Olier, R., and Volta, J. C., *J. Catal.* **145**, 318 (1994).
18. Eon, J.-G., Pries de Oliveira, P. G., Lefebvre, F., and Volta, J.-C., *Stud. Surf. Sci. Catal.* **82**, 83 (1994).
19. Batiot, C., and Hodnett, B. K., *Appl. Catal. A* **137**, 179 (1996).
20. Cassidy, F. E., and Hodnett, B. K., *CATTECH* **2**, 173 (1998).
21. Argyle, M. D., Chen, K. D., Bell, A. T., and Iglesia, E., *J. Phys. Chem. B*, in press.
22. Barton, D. G., Shtein, M., Wilson, R. D., Soled, S. L., and Iglesia, E., *J. Phys. Chem. B* **103**, 630 (1999).
23. Xie, S., Iglesia, E., and Bell, A. T., *Langmuir* **16**, 7162 (2000).
24. Iglesia, E., Baumgartner, J. E., and Price, G. L., *J. Catal.* **134**, 549 (1992).
25. Olthof, B., Khodakov, A., Bell, A. T., and Iglesia, E., *J. Phys. Chem. B* **104**, 1516 (2000).
26. Wachs, I. E., *Catal. Today* **27**, 437 (1996).
27. Vuurman, M. A., and Wachs, I. E., *J. Phys. Chem.* **96**, 5008 (1992).
28. Centi, G., *Appl. Catal. A* **147**, 267 (1996).
29. Chen, K. D., Bell, A. T., and Iglesia, E., *J. Phys. Chem. B* **104**, 1292 (2000).
30. Chen, K. D., Xie, S., Iglesia, E., and Bell, A. T., *J. Catal.* **189**, 421 (2000).
31. Chen, K. D., Iglesia, E., and Bell, A. T., unpublished results.
32. Sayle, D. C., Catlow, C. R. A., Perrin, M. A., and Nortier, P., *Catal. Lett.* **38**, 203 (1996).